HHS Public Access

Author manuscript

Acta Biomater. Author manuscript; available in PMC 2020 July 20.

Published in final edited form as:

Acta Biomater. 2020 January 01; 101: 586–597. doi:10.1016/j.actbio.2019.10.039.

Wear particles induce a new macrophage phenotype with the potential to accelerate material corrosion within total hip replacement interfaces

Divya Rani Bijukumar[1], **Shruti Salunkhe**[1], **Guoxing Zheng**[1], **Mark Barba**[1], **Deborah J. Hall**[3], **Robin Pourzal**[3], **Mathew T. Mathew**[1,2,*]

[1]Department of Biomedical Science, University of Illinois College of Medicine at Rockford, Rockford, IL

[2]Orthoillinois, Rockford, IL

[3]Department of Orthopedic Surgery, Rush University Medical Center, Chicago, IL

Abstract

Evidence that macrophages can play a role in accelerating corrosion in CoCrMo alloy in total hip replacement (THR) interfaces leads to questions regarding the underlying cellular mechanisms and immunological responses. Hence, we evaluated the role of macrophages in corrosion processes using the cell culture supernatant from different conditions and the effect of wear particles on macrophage dynamics. Monocytes were exposed to CoCrMo wear particles and their effect on macrophage differentiation was investigated by comparisons with M1 and M2 macrophage differentiation. Corrosion associated macrophages (M_{CA} macrophages) exhibited upregulation of TNF-α, iNOS, STAT-6, and PPARG and down-regulation of CD86 and ARG, when compared to M1 and M2 macrophages. M_{CA} cells also secreted higher levels of IL-8, IL-1β, IL-6, IL-10, TNF-α, and IL-12p70 than M1 macrophages and/or M2 macrophages. Our findings revealed variation in macrophage phenotype (M_{CA}) induced by CoCrMo wear particles in generating a chemical environment that induces cell-accelerated corrosion of CoCrMo alloy at THR modular interfaces.

Graphical Abstract

[*]**Corresponding author:** Mathew T. Mathew, University of Illinois College of Medicine at Rockford, 1601 Parkview Avenue, Rockford, IL 61107, Phone: +1 815 395 5883, mtmathew@uic.edu.

Author contributions

D.B and S.S equally contributed to the research work with the assistance of G.Z. The electrochemical experiments conducted were supervised by MTM and RP. MTM, DB, RP, DH initiated and coordinated this research and wrote the manuscript supported by SS. All authors discussed the results and contributed to the final version of the manuscript.

Competing interests

The authors declare no competing interests.

Declaration of interests

The authors declare that they have no known competing financial interests or personal relationships that could have appeared to influence the work reported in this paper.

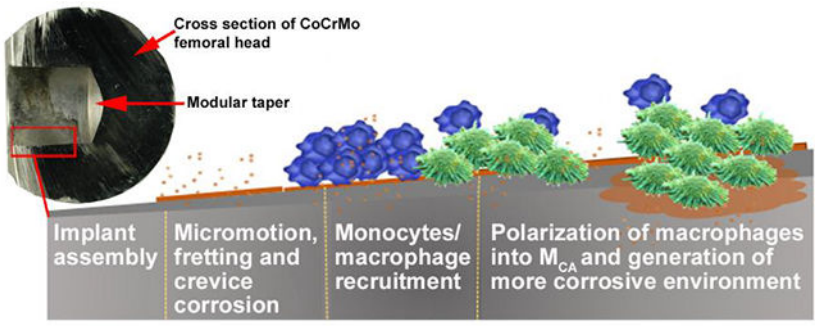

Keywords

monocytes; macrophage polarization; corrosion; CoCrMo; electrochemical impedance spectroscopy (EIS); modular junction; THR; gene expression

1.0 Introduction

Total hip replacement (THR) is one of the most common and successful medical procedures[1]. Yet, of the 332,000 THR procedures performed in the United States in 2017, 8.6% will require revision, according to statistics from the American Joint Replacement Registry[2]. Among the main factors leading to implant failure are infection, instability, and foreign body reactions to wear debris and corrosion products from the implant[3–5]. Fretting wear and corrosion within the implant's modular taper junction are prominent causes of implant failure, as they promote the release of corrosion products and subsequent development of adverse local tissue reactions [6]. Being a multifactorial process, several *in vitro* models have been developed to recreate the *in vivo* corrosion process, often described as mechanically-assisted crevice corrosion. Considering the excellent corrosion properties of CoCrMo alloy, the severity of chemically-generated damage observed at the modular interface has been surprising and poorly understood. Recent reports by Hall *et al.* showed cell-like features with trailing patterns at the taper interface of the modular junctions of retrieved implants[7,8], suggesting the possible involvement of cells in accelerating corrosion. Also, severe corrosion damage such as pitting, intergranular corrosion, and localized etching have been observed, which points to an aggressive chemical attack. In our previous study, we provided substantial *in vitro* evidence for cell-accelerated corrosion (CAC), highlighting the prominent role of macrophages in producing a corrosive chemical environment[9]. Furthermore, we found that macrophages can alter the chemical environment in the presence of wear debris generated from CoCrMo alloy and compromise the corrosion properties of CoCrMo alloy. However, the cellular mechanisms underlying CAC remain unknown.

As phagocytic cells located in peripheral tissues, macrophages play a diverse role in both physiological processes and pathological conditions[10]. They are a heterogeneous population of cells with major functions in inflammation, infection, phagocytosis, host defense, and tissue remodeling[11–14]. They respond rapidly to biomaterial implantation products in both soft and hard tissues[15]. Macrophages are highly plastic and can differentiate into different phenotypic subsets[16]. Depending upon various environmental stimuli, macrophages exhibit

different phenotypes[17,18]. Two major phenotypes are: classically-activated macrophages known as M1 macrophages and alternatively-activated macrophages known as M2 macrophages[19]. M1 macrophages are immune effector cells with an acute inflammatory phenotype[20,21], which are activated following infection or injury. They are highly aggressive against bacteria and produce large quantities of cytokines[21], especially pro-inflammatory cytokines, such as tumor necrosis factor (TNF)-α, interleukin (IL)-1β, IL-6, and IL-12. M1 macrophages also produce high levels of reactive oxygen and nitrogen species[22]. Conversely, M2 macrophages are immunosuppressive and assist in bone regeneration and tissue repair. They are characterized by the production of anti-inflammatory cytokines, such as IL-4, IL-13, IL-10, IL-1ra, C-C motif chemokine ligand (CCL)18, and CCL22[23], as well as low levels of reactive oxygen and nitrogen species[19]. In addition to M1 and M2 macrophages, Tatano *et al.* identified polarization of a novel population of macrophages (provisionally called *M17 macrophages*) in response to mycobacterial infection[24]. These cells exhibited markedly increased IL-17 production, leading to upregulated T-helper cell 17 (Th17) polarization. These reports provide evidence of multifarious polarization capacity of monocytes/macrophages *in vivo*.

1.1 Macrophage polarization by nanomaterials

Nanoparticles are also key signaling factors, which can modulate macrophage reprogramming[25], depending on their chemistry, size, and shape. Their varying effects are primarily attributed to differences in the cellular entry mechanism adopted by different nanoparticles. M1 and M2 polarization of various nanoparticles, such as Ag,[26–29] Au,[30] WC-Co,[31] ZnO,[32–34] TiO_2,[35] SiO_2,[28,36,37] and superparamagnetic iron oxide nanoparticles[38–40], have been studied. Polarized macrophages differ from each other on the basis of receptor expression, effector function, and cytokine and chemokine production[20,41,42]. The key feature of polarized macrophages is their differential cytokine production. Although the role of macrophages in corrosion of the modular junction of CoCrMo alloy in THR has been reported, their polarization at the corroded head-taper interface remains poorly understood[7,43–45]. CoCrMo wear particles, which are mostly within the nanometer-range (10–100 nm in diameter), but can also reach the micrometer-scale, are the major component released during fretting corrosion at the head-neck taper interface of a modular THR implant. Actual particle chemistry can vary. The majority of particles appear to be chromium oxide, but alloy particles, chromium phosphate, and metallo-organic complexes have also been reported.[46] Our group has previously established the differential response by the processed and unprocessed states of degradation products obtained from hip simulator in inducing neurodegeneration[47]. Hence, it is imperative to study the differentiation of macrophages in response to the clinically relevant wear particles to improve our understanding of macrophage action at the taper interface.

The aim of the current study is to provide a better understanding of macrophages and their plasticity at the THR taper interface when they encounter wear debris from CoCrMo alloy. This is a preliminary study along the path towards determining the mechanism(s) of CAC. In this study, the phenotype of wear particle–polarized (M_{CA}) macrophages is compared to the phenotypes of M1 and M2 macrophages. In addition, an electrochemical study of metal corrosion was conducted using the cell secreted media conditions from M1, M2 and M_{CA}.

2.0 Methods

2.1 Wear particles generation

Wear particles were generated from CoCrMo alloy samples using a tribocorrosion hip simulator with a pin-on-flat configuration. The samples were made of low carbon (<0.05%) wrought Co28Cr6Mo7 alloy (Carpenter Technology Ltd., PA, USA) as specified in ASTM F1537. The grain size of the alloy was 5.6 μm ± 3.6 μm (excluding twin boundaries). This alloy is typically used in orthopedics—most commonly for femoral heads of total hip replacements with a diameter of 28, 32 or 36mm. Tribocorrosion experimental conditions were developed and optimized previously by Mathew *et al.* (Figure 1a)[48]. The tribocorrosion hip simulator set-up consisted of a double-walled electrolyte chamber with a heated water bath system to maintain a constant solution temperature of 37°C. Contact between the hip head and cup was simulated through a pin-on-ball tribosystem, in which the pin (11-mm diameter, 7-mm thick) was made of CoCrMo alloy, and the ball was made of Al_2O_3 (28-mm diameter). The ball was placed in contact with the CoCrMo pin, which was supported by a polymeric pin holder. The pin had an exposed area of 0.95 cm^2 and acted as the working electrode (WE). A graphite rod (counter electrode [CE]) and standard calomel electrode (reference electrode [RE]) were immersed in the electrolyte solution, to create a three-electrode electrochemical system. To maintain uniformity, the positions of the electrodes were kept constant inside the chamber throughout the study. A load of 16 N was applied as the ball articulated on the flat CoCrMo surface. The rotation frequency was set at 1 Hz and the amplitude was set at 30 degrees, for a total sliding duration of 750,000 cycles. A 16-N load was chosen to achieve a physiologically relevant initial Hertzian contact pressure of 480 MPa. As the purpose of this study was to generate particles under physiologically relevant conditions, the tribocorrosion tests were conducted under free potential conditions (open circuit potential [OCP] was monitored) for 750,000 cycles using an electrolyte solution based on bovine calf serum (BCS; 30 g protein/L BCS diluted with buffer contains NaCl (9g/L, Fisher Bioreagents, Cat#BP358–1), EDTA (200mg/L, Fischer Chemical, Cat#E478–500) and Tris (27g/L, Acros chemicals Cat#167620010) at pH 7.4 and with added 100 IU/mL of penicillin/streptomycin antibiotics (Corning, Cat #MT30009CI) during the production of CoCrMo wear particles. The applied load, angle of rotation of the ball (amplitude of oscillations), and torque were monitored using LabView software (Loadstar Ltd, CA). The electrolyte solution was kept at a constant volume of 150 mL (by adding 4–5 mL of fresh solution per day to compensate for evaporation) and a constant pH of 7.6 throughout the tribocorrosion tests. The wear particles were collected after 750,000 cycles and centrifuged at 12,000 rpm for 20 minutes. The supernatant was then discarded, and the pellet was re-suspended in distilled water. A particle concentration of 12mg/ml was obtained from the dry weight of 1ml of the aliquot from the stock. The original stock solution was stored at −20°C and an aliquot of stock was refrigerated at 4°C (0–4 months) until use. The endotoxin levels of the particle samples were checked prior to cell culture tests[47].

2.2 Cell culture

Human monocyte (THP-1) cells were cultured in Roswell Park Memorial Institute (RPMI) 1640 (Corning, Cat#MT10041CM)) media containing 10% fetal bovine serum (FBS; Gibco, Cat#10082139) and 100 IU/ml of Penicillin-Streptomycin antibiotics (10,000 IU/ml, Gibco,

#15140122, USA). THP-1 monocytes were treated with 5 ng/mL PMA (Sigma, P1585) for 24 h. Further, the cells were treated in three different conditions 1) M1 macrophages by incubating with, 20 ng/mL IFN-γ (R&D systems, Cat# 285-IF-100), and 10 pg/mL LPS (Sigma, #8630), 2) M2 polarization by incubating cells with 20 ng/mL IL-4 (R&D Systems, Cat#204-IL-010)), and 20 ng/mL IL-13 (R&D Systems, Cat#213-ILB-005)[49] and, 3) M_{CA} cells were generated by treating CoCr wear particles at a concentration of 1 μg/mL to M0 macrophages for a period of 24 hours (Figure 2a). The concentration of wear particles was chosen based on the dose-dependent toxicity evaluation reported in our previous studies on neuronal cells[47], monocytes, macrophages and osteoblast cells[9]. The results from the previous study showed that the concentration of wear particles required to challenge the monocytes and macrophages with >88% viability after 24 hours was 1 μg/ml.[9]

2.3 Reactive oxygen species assay

THP-1 monocytes were seeded at 100,000 cells/well in a 24-well plate and differentiated as described above. M1 and M2 cells were then incubated with fresh media for 3 hours after completion of the differentiation protocols described in section 2.2. M0 cells were treated with 1 μg/mL of wear particles for 3 hours (M_{CA}). For comparison THP-1 cells also incubated with 3h fresh media. After incubation all the cell cultures were trypsinized and triturated to obtain a cell suspension. The suspension was centrifuged at 3000 rpm at room temperature for 3 minutes. The cell pellet was then resuspended in 1 mL fresh RPMI 1640 medium. The cells were then incubated with ROS dye (H2DCFDA, Tocris Bioscience, Cat#59–351-00) for 1 hour and then analyzed by flow cytometry using FACScalibur (BD Biosciences).

2.4 Gene expression analysis

RT-qPCR was used to determine gene expression to confirm expression of M1 and M2 macrophages and to characterize the expression of M_{CA} macrophages. A total of 100,000 THP-1 monocytes were seeded in a 24-well plate, followed by the differentiation to M1 and M2 macrophages. After differentiation, cells were incubated for another 48 hours before harvesting for RNA isolation. The M0 macrophages were treated with wear particles for 24 hours to generate M_{CA} prior to RNA isolation. Total RNA was extracted using the Trizol method (Trizol reagent, Invitrogen, Cat # 15596026). One microgram of total RNA was reverse transcribed using a reverse transcription kit (Applied biosystems, Cat#4374966). The relative gene expression of TNF-α, iNOS 2, and CD86 for M1 macrophages and ARG, MRC, PPARG, and STAT 6 for M2 macrophages were carried out with Power Up SYBR Green master mix (Applied Biosystems, Cat # A25742). GAPDH was used as the reference gene for normalization. All the pre-designed primers were purchased from Sigma Aldrich. The primer sequence, gene ID and the primer efficiencies were presented in the supplementary data (Table S1). The results were quantified by evaluating the relative mRNA expression (2^{-dCT}) normalized with GAPDH expression levels of each condition. The data is presented as mRNA expression relative to GAPDH. RT-qPCR was performed using the Applied Biosciences by Life Technologies qPCR QuantStudio ™ 7.

2.5 Cytokine bead array

To better understand cytokine expression by M_{CA} macrophages, we performed a cytokine bead array experiment. A total of 100,000 cells were seeded in a 24-well plate and differentiated as described above. The concentration of a panel of cytokines, including IL-8, IL-1β, IL-6, IL-10, TNF-α, and IL-12p70, was determined using the BD CBA Human Inflammatory Cytokines Kit, according to the manufacturer's instructions (BD Biosences, Cat#BDB552932). All data were analyzed using FCAP Array V3 software (BD Biosciences).

2.6 Electrochemical studies

CoCrMo alloy discs with an exposed area of 0.95 cm^2 were mounted onto a custom-made polysulfonate multi-well corrosion chamber (Figure 2b). CoCrMo alloy samples polished with 320-grit silicon carbide paper were connected to a single channel of an electrochemical multiplexer, which was controlled by the Grammy interface 1000E potentiostat in a three-electrode configuration. The setup included a RE (standard calomel electrode), a CE (graphite rod), and a WE (CoCrMo alloy sample). The analysis sequence was as follows: OCP-1, potentiostatic scan, OCP-2, electrochemical impedance spectroscopy (EIS), cyclic polarization, and OCP3. All measurements were conducted at room temperature using different media as the electrolyte solutions: media of the respective cell cultures (10^5 cells) after 24-h incubation of M1 (M0 macrophages treated with M1 differentiation specific growth factors) and M2 (M0 macrophages treated with M2 differentiation specific growth factors) and M_{CA} (M0 macrophages treated with wear particles) macrophages.

OCP, EIS, and potentiodynamic polarization data were used to determine the corrosion tendency, I_{corr}, and corrosion kinetics. The potentiodynamic tests were performed at 0.8–1.8 V vs the standard calomel electrode (the RE), with a scan rate of 1 mV/s. The corrosion tendency and corrosion potential were derived from the potentiodynamic data. EIS tests were performed at OCP at a frequency of 100 kHz–0.01 Hz, with an amplitude of ± 10mV. A modified Randle's circuit was used as an equivalent electrical circuit to model the EIS data, from which the resistance to polarization and capacitance were determined.

2.7 Scanning electron microscopy

Cell like features that were earlier observed[7] on a retrieved femoral head were further analyzed. Scanning electron microscopy (SEM) images were obtained from this severely corroded modular head taper made from wrought CoCrMo alloy. This component was removed from the patient for pain and instability after 2 years *in situ*. The taper surface was imaged using secondary electron emission with accelerating voltages of 5kV, 10kV, and 20 kV at magnifications between 250x and 4500x (JSM 6490 LV, JEOL, Peabody, MA). The taper section was sputter coated with gold/palladium (80:20) at a thickness of approximately 4 nm to prevent charging of the cell-like features and thus improving the image quality.

2.8 Statistical analyses

Student's t-test was used, and a p-value < 0.05 was considered significant in all statistical tests. The samples were examined for significance by comparisons to the control samples.

3.0 Results

3.1 Macrophage differentiation

Microscopic observations showed that, upon treatment with 5 ng/mL phorbol 12-myristate 13-acetate (PMA) for 24 hours, the human monocyte-like cells (THP-1) adhered to the surface of the culture flask and changed their morphology, becoming M0 macrophages. Upon treatment with M1 macrophage differentiating factors (lipopolysaccharide [LPS] and interferon [INF]-γ), the cells circularized and displayed M1 macrophage–like morphology. Upon treatment with M2 macrophage growth factors (IL-4 and IL-13), the cells spread out and displayed fibroblast-like morphology (Figure 2b(i)). The cells treated with wear particles also became adherent, and spread out with a different morphology closer to M1 than M2. The cells were maintained in culture for 24–48 hours before performing further experiments. The shape factor (W/L ratio) of cells at different conditions was quantified by image J software to further understand the difference in morphology. A significant difference in W/L ratio was observed in the case of M0, M1 and M2 macrophages. The M_{CA} macrophages showed an intermediate morphology in comparison to M1 and M2 macrophages (Figure 2b(ii)).

3.2 Production of reactive oxygen species by polarized macrophages

Flow cytograms showed live cell populations and cells expressing reactive oxygen species (ROS) (Figure 3). M1 macrophages exhibited higher ROS levels than THP-1 monocytes and M2. The ROS expression of M_{CA} macrophages was observed to be intermediate between M2 and M1 macrophages after 3 hours of wear particle exposure.

3.3 Relative mRNA expression profiles of polarized macrophages

Upon differentiating THP-1 monocytes into M1 and M2 macrophage lineages, gene expression analysis was performed to confirm the phenotype of each lineage. Expression of CD86 and inducible nitric oxide synthase (iNOS) was significantly higher in M1 macrophages than in M2 macrophages ($p<0.05$). Even though TNF-α had a higher value in M1 compared to M2 there was no statistically significant difference in expression between them. Cells treated with M2-specific factors showed significantly higher expression of peroxisome proliferator-activated receptor gamma (PPARG), mannose receptor (MRC), and arginase (ARG) ($p<0.05$) than macrophages differentiated with M1-specific factors. Signal transducer and activator of transcription 6 (STAT6) expression did not differ between macrophages differentiated with M1- or M2-specific factors. These results confirmed the differentiation of monocytes into M1 and M2 macrophages (Figure 4a).

M_{CA} macrophages exhibited significantly higher expression of TNF-α and iNOS (M1 marker genes) than cells differentiated with M1- or M2-specific factors. M_{CA} macrophages exhibited a significantly lower expression of CD86 than M1 macrophages, as well as significantly higher STAT-6 expression than both M1 and M2 macrophages. M_{CA} macrophage expression of PPARG and MRC was comparable to PPARG and MRC expression in M2 and M1 macrophages, respectively. ARG expression was significantly lower in M_{CA} macrophages than in M1 and M2 macrophages (Figure 4b).

3.4. Cytokine profiles of M1, M2, and M_{CA} macrophages

Standard curves were derived for concentrations ranging from 20 to 5000 pg/mL and 0 to 20 pg/mL to determine the levels of cytokines released by M_{CA} macrophages and to compare these levels to the levels of cytokines released from M1 and M2 macrophages. IL-8 showed increased levels in both control conditions (M1 and M2 macrophages) and test conditions (M_{CA} macrophages). Significantly higher levels of IL-1β and TNF-α were released from M_{CA} macrophages than from both M1 and M2 macrophages. In the case of IL-10, the cytokine released from M1 and M2 macrophages was below the detection limit of 3.3pg/ml of the test kit. However, a significant increase in IL-10 was observed in MCA cells (5.66±0.97pg/ml) compared to M1 and M2 macrophages. Overall, the cytokine profile of M_{CA} macrophages was observed to be different from the cytokine profiles of M1 and M2 macrophages (Figure 5).

3.5 Corrosion rates and kinetics of CoCrMo metal exposed to M1, M2, and M_{CA} secretory products

The evolution of the open circuit potential (OCP) as a function of time showed low potential values for supernatants from M1 and M_{CA} macrophages, when compared to the supernatant from M2 macrophages (Figure 6a). The corrosion rate (I_{corr}), obtained from the Tafel's plot of cyclic polarization data, was higher with supernatant from M_{CA} macrophages than with supernatants from M1 and M2 macrophages (Figure 6b & c). Resistance to polarization was lowest with M1 macrophage supernatant, indicating that this media produced the highest corrosion kinetics. Corrosion kinetics were higher (i.e., lower resistance value) with the supernatant from M_{CA} macrophages than with the supernatant from M2 macrophages (Figure 6d). Little variability in capacitance was observed between supernatants from the three types of macrophages (Figure 6e). The variation in Rp and C may be attributed to the discrepancies in the goodness fit parameters of the EIS equivalent circuit. A satisfied goodness of fit below 0.001 was expected in the EIS modeling simulation, however, in the biomedical applications, many factors can influence the corrosion kinetics and subsequent data and model.

4.0 Discussion

4.1 Cell-accelerated corrosion (CAC): what we knew and what we have learned

The purpose of this study was to identify the cellular mechanisms leading to CAC in THR modular taper junctions by determining the phenotype, function, and differentiation of macrophages upon exposure to wear particles generated from CoCrMo alloy. Changes in macrophage dynamics provide insights into the cellular mechanisms of CAC. Previous findings from *in vitro* experiments[9] suggested that amongst the periprosthetic cell populations, macrophages have a prominent impact, generating a corrosive environment. The results showed an increase in corrosion kinetics and rate of corrosion of CoCrMo alloy when exposed to media produced by macrophages challenged with wear particles. Our earlier retrieval findings demonstrated the presence of cell-like features on the head taper surface of femoral heads that were removed after several years in situ[7]. The size of 10 to 20 micrometers and morphology of these cell-like features can be indicative of macrophages (Figure 7). Scanning electron microscopic images (SEM) of retrieved femoral heads have

shown that a large amount of cells appeared to populate areas of the head taper surface in areas that were previously in contact with the stem taper of the femoral stem (Figure 7A, B, C), thus proving that cells can enter the crevice. Some cells even appeared to leave a trail on the metal surface (Figure 7B). A closer look at these etching trails revealed typical microstructural features of wrought CoCrMo alloy such as twin boundaries and slip bands (Figure 7D). Such features are usually only exposed by metallographic sample preparation that usually involves etching within acidic solutions. Its occurrence on a retrieved implant is remarkable, and hints to a strong chemical attack *in vivo.* The combination of our previous experimental and implant retrieval findings prompted us to further investigate the cellular mechanisms employed by macrophages to accelerate implant damage.

Our group has previously demonstrated the physicochemical characteristics of CoCrMo wear particles generated in a hip simulator compared to processed wear particles[47]. In addition, a detailed investigation on the differential response of neurons towards processed and as-synthesized particles clearly demonstrated the higher toxicity levels of as-synthesized particles from hip simulator. Moreover, it was previously reported that there is a dose dependent toxicity induced by wear particles to the neurons, monocytes, macrophages and osteoblasts[47]. The current study revealed the possible ways by which wear particles generated from CoCrMo alloy can affect macrophage dynamics. Based on the results of similar studies, it has been previously speculated that cell-mediated corrosion of CoCrMo is primarily associated with the generation of ROS, which leads to Fenton-like reactions. However, Fenton-like processes are extremely complex, predominantly driven by oxidizing intermediate radicals, and sensitive to changes in chemical and biological environments[50], such as cellular secretions and the chemistry of materials at the cell-material interface. Furthermore, the lower level of ROS produced by M_{CA} macrophages, compared to M1 macrophages (Figure 3d), did not correlate with the higher rate of corrosion (I_{corr}: 0.753 ± 0.04 μA/cm^2, Figure 5c) with M_{CA} macrophages, compared to M1 (I_{corr}: 0.052 ± 0.03 μA/cm^2) and M2 ($I_{corr:}$ 0.025 ± 0.001 μA/cm^2) macrophages. These observations suggest that Fenton-like reactions may not be the only factor in inflammatory cell–accelerated corrosion. Thus, additional mechanism(s) must be acting at the cell-material interface to account for the unexpectedly accelerated rate of corrosion.

Macrophages are a heterogeneous population of cells exhibiting different phenotypic characteristics under the influence of various stimuli[23,42,51]. Resting (M0) macrophages can be reprogramed to M1 or M2 macrophages by internalizing endogenous or exogenous materials, such as foreign pathogens (bacteria and viruses), cells, cellular debris, and other material[14,52]. Reprogramming occurs through evolutionarily conserved pattern recognition receptors that sense and recognize pathogenic factors, thereby initiating an immune response[53,54]. Primary tissue macrophages do not readily expand *ex vivo*, so monocytic cell lines are usually used to model macrophage functions[55]. Hence, for this study, we used a monocytic cell line to study the effects of CoCrMo nanoparticles on the polarization of THP-1-differentiated macrophages. Classically-activated M1 macrophages and alternatively-activated M2 macrophages were used as controls to determine the phenotype of M_{CA} macrophages (cells differentiated through exposure to CoCrMo wear debris), which was confirmed by examining the gene expression profile of M1- and M2-specific markers (Figure 4). During these experiments, we observed increased expression of TNF-α and

iNOS (M1 markers) and decreased MRC (M2 marker) expression in M_{CA} macrophages, suggesting polarization towards the M1 phenotype. However, M_{CA} macrophages also exhibited higher expression of STAT-6 and PPARG (M2 markers) than M2 macrophages and lower CD86 (M1 marker) expression than M1 macrophages, suggesting that M_{CA} macrophages may have features of M2 macrophages as well. These findings contrast with those of previous studies, in which nanoparticle-mediated polarization of macrophages was towards either the M1 or M2 phenotype. Thus, based on the marker genes evaluated, our experiments (which were repeated six separate times) shows the higher probability of polarization of the wear particle induced macrophages (M_{CA} macrophages) in comparison to M1 or M2 phenotype. Further detailed investigation on specific phenotype markers by gene transcript and surface marker analysis is required to make conclusion.

Although macrophages could have different characteristics under the influence of wear particles *in vitro* than *in vivo*, our results provide insight into possible mechanisms of CAC. The site of an implant contains a mixed population of resident macrophages and macrophages recruited by the presence of wear debris. Based on the results and the observed cells at the taper interface, it can be suggested that monocytes recruited to the implant site by inflammation or resident macrophages (M0 macrophages) in the surrounding tissue can be activated by wear debris. Differentiation of monocytes or M0 macrophages occurs under these stress conditions, with the differentiated macrophages polarizing to M_{CA} macrophages (Figure 8). It is also possible that M1 or M2 macrophages may be reprogrammed to M_{CA} macrophages, which needs to be investigated in further detail. Yet, the differences in gene expression, ROS production, cytokine profiling, and electrochemical properties of secreted products clearly indicate that M_{CA} macrophages are distinct from both M1 and M2 macrophages and may play a key role in CAC by altering the chemical environment within the confined space of the modular THR taper junction.

4.2 Limitations and future directions

One of the limitation of this study is the use of THP-1 cell lines. There can be some difference in the expression profile by the THP-1 cells in comparison to peripheral blood mononuclear cells. We acknowledge that a limited number of genes and cytokines were selected for profiling in this study. Complete profiling of macrophage pro-inflammatory and anti-inflammatory cytokines and genes is important to provide more insight into the macrophage phenotype induced by wear particles generated from CoCrMo alloy. However, our results suggest that macrophages in the presence of CoCrMo wear particles have different phenotypic characteristics when compared to M1 and M2 macrophages. Possible signaling pathways involved in the phenotypic changes also require evaluation. As the plasticity of cells at the modular THR taper interface may vary, and the subsequent effects are poorly understood, it is imperative to understand the cell signaling pathways triggered by the presence of wear particles. Such analysis may assist in determining the exact cellular mechanisms and immunological response associated with CAC. We also would like to acknowledge that we have not analyzed the metal ion dissolution during the storage of the CoCrMo particles at 4°C.

5.0 Conclusions

In conclusion, our findings describe a variation in phenotype of macrophages that could be recruited to the modular taper interface of a THR and how these cells may contribute to the corrosion process *in vivo*. In the presence of wear particles from the CoCrMo surface, macrophages at the site of the interface could polarize into M_{CA} macrophages, which are newly characterized in this report. This study also confirmed that the corrosive environment created by M_{CA} macrophages contains not only ROS but also inflammatory cytokines. Both ROS and cytokines may activate electrochemical changes at microstructure level that drive the passivation and preferential dissolution processes at the surface of the alloy, thus accelerating damage caused by corrosion.

Supplementary Material

Refer to Web version on PubMed Central for supplementary material.

Acknowledgments

The authors acknowledge financial support from NIH grant R01 AR070181 and funding provided by the Blazer Foundation for the Regenerative Medicine and Disability Research Lab (RMDR) at the Department of Biomedical Sciences, UIC College of Medicine at Rockford. Editorial support was provided by the Rush Research Mentoring Program. The authors thank Dr. H. Lundberg, Dr. R. Urban, Dr. Wimmer, Dr. J. Jacobs at (Rush University Medical Center) Prof. A. Fischer (University Duisburg) and Prof. K Shull (Northwestern University) for the valuable suggestion/comments and mentorship. We also acknowledge the help of Ms. Oba Akinfosile, Ms. R. Nagaraj and Ms. O. Kerr.

References

1. Katz JN, Wright EA, Polaris JJ, Harris MB & Losina E Prevalence and risk factors for periprosthetic fracture in older recipients of total hip replacement: a cohort study. BMC Musculoskelet. Disord. 15, 168 (2014). [PubMed: 24885707]
2. Registry AJR Download the AJRR 2017 Annual Report. Available at: http://connect.ajrr.net/2017-annual-report-download. (Accessed: 31st May 2018)
3. Sansone V, Pagani D & Melato M The effects on bone cells of metal ions released from orthopaedic implants. A review. Clin. Cases Miner. Bone Metab. 10, 34–40 (2013). [PubMed: 23858309]
4. Franz S, Rammelt S, Scharnweber D & Simon JC Immune responses to implants – A review of the implications for the design of immunomodulatory biomaterials. Biomaterials 32, 6692–6709 (2011). [PubMed: 21715002]
5. Ulrich SD, Seyler TM, Bennett D, Delanois RE, Saleh KJ, Thongtrangan I, Kuskowski M, Cheng EY, Sharkey PF, Parvizi J and Stiehl JB, Total hip arthroplasties: What are the reasons for revision? Int. Orthop. 32, 597–604 (2008). [PubMed: 17443324]
6. Hoeppner DW & Chandrasekaran V Fretting in orthopaedic implants: A review. Wear 173, 189–197 (1994).
7. Hall DJ, Pourzal R, Lundberg HJ, Mathew MT, Jacobs JJ and Urban RM Mechanical, chemical and biological damage modes within head-neck tapers of CoCrMo and Ti6Al4V contemporary hip replacements. J. Biomed. Mater. Res. B Appl. Biomater. 106, 1672–1685 (2018). [PubMed: 28842959]
8. Hall D, Pourzal R, Della Valle C, Galante J, Jacobs J and Urban R Corrosion of Modular Junctions in Femoral and Acetabular Components for Hip Arthroplasty and Its Local and Systemic Effects. Modul. Tapers Total Jt. Replace. Devices (2015). doi:10.1520/STP159120140134.
9. Bijukumar DR, Salunkhe S, Morris D, Segu A, Hall DJ, Pourzal R, Mathew MT In Vitro Evidence for Cell-Accelerated Corrosion within Modular Junctions of Total Hip Replacements. J. Orthop. Res. doi.org/10.1002/jor.24447, (2019).

10. Sica A & Mantovani A Macrophage plasticity and polarization: in vivo veritas. J. Clin. Invest. 122, 787–795 (2012). [PubMed: 22378047]
11. Hill AA, Bolus WR & Hasty AH A decade of progress in adipose tissue macrophage biology. Immunol. Rev. 262, 134–152 (2014). [PubMed: 25319332]
12. Oberdörster G, Ferin J & Lehnert BE Correlation between particle size, in vivo particle persistence, and lung injury. Environ. Health Perspect. 102, 173–179 (1994).
13. Zanganeh S, Hutter G, Spitler R, Lenkov O, Mahmoudi M, Shaw A, Pajarinen JS, Nejadnik H, Goodman S, Moseley M and Coussens LM Iron oxide nanoparticles inhibit tumour growth by inducing pro-inflammatory macrophage polarization in tumour tissues. Nat. Nanotechnol. 11, 986–994 (2016). [PubMed: 27668795]
14. Mosser DM & Edwards JP Exploring the full spectrum of macrophage activation. Nat. Rev. Immunol. 8, 958–969 (2008). [PubMed: 19029990]
15. Xia Z & Triffitt JT A review on macrophage responses to biomaterials. Biomed. Mater. 1, R1 (2006). [PubMed: 18458376]
16. Daigneault M, Preston JA, Marriott HM, Whyte MKB & Dockrell DH The Identification of Markers of Macrophage Differentiation in PMA-Stimulated THP-1 Cells and Monocyte-Derived Macrophages. PLOS ONE 5, e8668 (2010). [PubMed: 20084270]
17. Mantovani A, Biswas SK, Galdiero MR, Sica A & Locati M Macrophage plasticity and polarization in tissue repair and remodelling. J. Pathol. 229, 176–185 (2013). [PubMed: 23096265]
18. Tarique AA, Logan J, Thomas E, Holt PG, Sly PD and Fantino E Phenotypic, Functional, and Plasticity Features of Classical and Alternatively Activated Human Macrophages. Am. J. Respir. Cell Mol. Biol. 53, 676–688 (2015). [PubMed: 25870903]
19. Martinez FO & Gordon S The M1 and M2 paradigm of macrophage activation: time for reassessment. F1000Prime Rep. 6, (2014).
20. Arango Duque G & Descoteaux A Macrophage Cytokines: Involvement in Immunity and Infectious Diseases. Front. Immunol. 5, (2014).
21. Liu Y-C, Zou X-B, Chai Y-F & Yao Y-M Macrophage Polarization in Inflammatory Diseases. Int. J. Biol. Sci. 10, 520–529 (2014). [PubMed: 24910531]
22. Tan HY, Wang N, Li S, Hong M, Wang X and Feng Y The Reactive Oxygen Species in Macrophage Polarization: Reflecting Its Dual Role in Progression and Treatment of Human Diseases. Oxidative Medicine and Cellular Longevity (2016). doi:10.1155/2016/2795090.
23. Gordon S Alternative activation of macrophages. Nat. Rev. Immunol. 3, 23–35 (2003). [PubMed: 12511873]
24. Tatano Y, Shimizu T & Tomioka H Unique macrophages different from M1/M2 macrophages inhibit T cell mitogenesis while upregulating Th17 polarization. Sci. Rep. 4, 4146 (2014). [PubMed: 24553452]
25. Miao X, Leng X & Zhang Q The Current State of Nanoparticle-Induced Macrophage Polarization and Reprogramming Research. Int. J. Mol. Sci. 18, 336 (2017).
26. Bastus N, Sánchez-Tilló E., Pujals S, Farrera C, Lopez C, Giralt E, Celada A, Lloberas J. and Puntes V. Homogeneous Conjugation of Peptides onto Gold Nanoparticles Enhances Macrophage Response. ACS Nano 3, 1335–1344 (2009). [PubMed: 19489561]
27. Zazo H, Colino CI, Warzecha KT, Hoss M, Gbureck U, Trautwein C, Tacke F, Lanao JM and Bartneck M Gold Nanocarriers for Macrophage-Targeted Therapy of Human Immunodeficiency Virus. Macromol. Biosci. 17, (2017).
28. Bancos S, Stevens DL & Tyner KM Effect of silica and gold nanoparticles on macrophage proliferation, activation markers, cytokine production, and phagocytosis in vitro. Int. J. Nanomedicine 10, 183–206 (2015).
29. Sarkar S, Leo BF, Carranza C, Chen S, Rivas-Santiago C, Porter AE, Ryan MP, Gow A, Chung KF, Tetley TD and Zhang JJ Modulation of Human Macrophage Responses to Mycobacterium tuberculosis by Silver Nanoparticles of Different Size and Surface Modification. PLOS ONE 10, e0143077 (2015). [PubMed: 26580078]
30. Bastús NG, Sánchez-Tilló E, Pujals S, Farrera C, Kogan MJ, Giralt E, Celada A, Lloberas J and Puntes V Peptides conjugated to gold nanoparticles induce macrophage activation. Mol. Immunol. 46, 743–748 (2009). [PubMed: 18996597]

31. Armstead AL & Li B In vitro inflammatory effects of hard metal (WC-Co) nanoparticle exposure. Int. J. Nanomedicine 11, 6195–6206 (2016). [PubMed: 27920526]
32. Belgiovine C, D'Incalci M, Allavena P & Frapolli R Tumor-associated macrophages and anti-tumor therapies: complex links. Cell. Mol. Life Sci. CMLS 73, 2411–2424 (2016). [PubMed: 26956893]
33. Wang J, Lee JS, Kim D & Zhu L Exploration of Zinc Oxide Nanoparticles as a Multitarget and Multifunctional Anticancer Nanomedicine. ACS Appl. Mater. Interfaces 9, 39971–39984 (2017). [PubMed: 29076344]
34. Roy R, Parashar V, Chauhan LKS, Shanker R, Das M, Tripathi A and Dwivedi PD Mechanism of uptake of ZnO nanoparticles and inflammatory responses in macrophages require PI3K mediated MAPKs signaling. Toxicol. Vitro Int. J. Publ. Assoc. BIBRA 28, 457–467 (2014).
35. Scherbart AM, Langer J, Bushmelev A, van Berlo D, Haberzettl P, van Schooten FJ, Schmidt AM, Rose CR, Schins RP Contrasting macrophage activation by fine and ultrafine titanium dioxide particles is associated with different uptake mechanisms. Part. Fibre Toxicol. 8, 31 (2011). [PubMed: 21995556]
36. Cejudo-Guillén M, Ramiro-Gutiérrez ML, Labrador-Garrido A, Díaz-Cuenca A & Pozo D Nanoporous silica microparticle interaction with toll-like receptor agonists in macrophages. Acta Biomater. 8, 4295–4303 (2012). [PubMed: 22842032]
37. Kwon D, Cha BG, Cho Y, Min J, Park EB, Kang SJ and Kim J Extra-Large Pore Mesoporous Silica Nanoparticles for Directing in Vivo M2 Macrophage Polarization by Delivering IL-4. Nano Lett. 17, 2747–2756 (2017). [PubMed: 28422506]
38. Laskar A, Eilertsen J, Li W & Yuan X-M SPION primes THP1 derived M2 macrophages towards M1-like macrophages. Biochem. Biophys. Res. Commun. 441, 737–742 (2013). [PubMed: 24184477]
39. Rojas JM, Sanz-Ortega L, Mulens-Arias V, Gutiérrez L, Pérez-Yagüe S and Barber DF Superparamagnetic iron oxide nanoparticle uptake alters M2 macrophage phenotype, iron metabolism, migration and invasion. Nanomedicine Nanotechnol. Biol. Med. 12, 1127–1138 (2016).
40. Kodali V, Littke MH, Tilton SC, Teeguarden JG, Shi L, Frevert CW, Wang W, Pounds JG and Thrall BD Dysregulation of Macrophage Activation Profiles by Engineered Nanoparticles. ACS Nano 7, 6997–7010 (2013). [PubMed: 23808590]
41. Mantovani A, Sica A, Sozzani S, Allavena P, Vecchi A and Locati M The chemokine system in diverse forms of macrophage activation and polarization. Trends Immunol. 25, 677–686 (2004). [PubMed: 15530839]
42. Gordon S & Taylor PR Monocyte and macrophage heterogeneity. Nat. Rev. Immunol. 5, 953–964 (2005). [PubMed: 16322748]
43. Hall D, Pourzal R, Della Valle C, Galante J, Jacobs J and Urban R Corrosion of Modular Junctions in Femoral and Acetabular Components for Hip Arthroplasty and Its Local and Systemic Effects. Modul. Tapers Total Jt. Replace. Devices (2015). doi:10.1520/STP159120140134.
44. Gilbert JL, Mali S, Urban RM, Silverton CD & Jacobs JJ In vivo oxide-induced stress corrosion cracking of Ti-6Al-4V in a neck-stem modular taper: Emergent behavior in a new mechanism of in vivo corrosion. J. Biomed. Mater. Res. B Appl. Biomater. 100, 584–594 (2012). [PubMed: 22113876]
45. Gilbert JL, Sivan S, Liu Y, Kocagöz SB, Arnholt CM and Kurtz SM Direct in vivo inflammatory cell-induced corrosion of CoCrMo alloy orthopedic implant surfaces. J. Biomed. Mater. Res. A 103, 211–223 (2015). [PubMed: 24619511]
46. Xia Z, Ricciardi BF, Liu Z, von Ruhland C, Ward M, Lord A, Hughes L, Goldring SR, Purdue E, Murray D and Perino G Nano-analyses of wear particles from metal-on-metal and non-metal-on-metal dual modular neck hip arthroplasty. Nanomedicine Nanotechnol. Biol. Med. 13, 1205–1217 (2016).
47. Bijukumar DR, Segu A, Mou Y, Ghodsi R, Shokufhar T, Barba M, Li XJ and Thoppil Mathew M Differential toxicity of processed and non-processed states of CoCrMo degradation products generated from a hip simulator on neural cells. Nanotoxicology (2018).

48. Mathew MT, Uth T, Hallab NJ, Pourzal R, Fischer A and Wimmer MA Construction of a tribocorrosion test apparatus for the hip joint: Validation, test methodology and analysis. Wear 271, 2651–2659 (2011).

49. Genin M, Clement F, Fattaccioli A, Raes M & Michiels C M1 and M2 macrophages derived from THP-1 cells differentially modulate the response of cancer cells to etoposide. BMC Cancer 15, (2015).

50. Goldstein S & Meyerstein D Comments on the Mechanism of the “Fenton-Like” Reaction. Acc. Chem. Res. 32, 547–550 (1999).

51. Mantovani A, Sozzani S, Locati M, Allavena P & Sica A Macrophage polarization: tumor-associated macrophages as a paradigm for polarized M2 mononuclear phagocytes. Trends Immunol. 23, 549–555 (2002). [PubMed: 12401408]

52. Chellat F, Merhi Y, Moreau A & Yahia L Therapeutic potential of nanoparticulate systems for macrophage targeting. Biomaterials 26, 7260–7275 (2005). [PubMed: 16023200]

53. Hoffmann JA, Kafatos FC, Janeway CA & Ezekowitz R. a. B. Phylogenetic Perspectives in Innate Immunity. Science 284, 1313–1318 (1999). [PubMed: 10334979]

54. Anderson KV Toll signaling pathways in the innate immune response. Curr. Opin. Immunol. 12, 13–19 (2000). [PubMed: 10679407]

55. Lunov O, Syrovets T, Loos C, Beil J, Delacher M, Tron K, Nienhaus GU, Musyanovych A, Mailander V, Landfester K and Simmet T Differential Uptake of Functionalized Polystyrene Nanoparticles by Human Macrophages and a Monocytic Cell Line. ACS Nano 5, 1657–1669 (2011). [PubMed: 21344890]

Statement of Significance

Fretting wear and corrosion within the implant's modular taper junction are prominent causes of implant failure, as they promote the release of corrosion products and subsequent development of adverse local tissue reactions. Being a multifactorial process, several *in vitro* models have been developed to recreate the *in vivo* corrosion process, often summarized as mechanically-assisted crevice corrosion. Considering the excellent corrosion properties of CoCrMo alloy, the severity of chemically-generated damage observed at the modular interface has been surprising and poorly understood. The aim of the current study is to provide a better understanding of macrophages and their plasticity at the THR taper interface when they encounter wear debris from CoCrMo alloy. This is a preliminary study along the path towards determining the mechanism(s) of CAC.

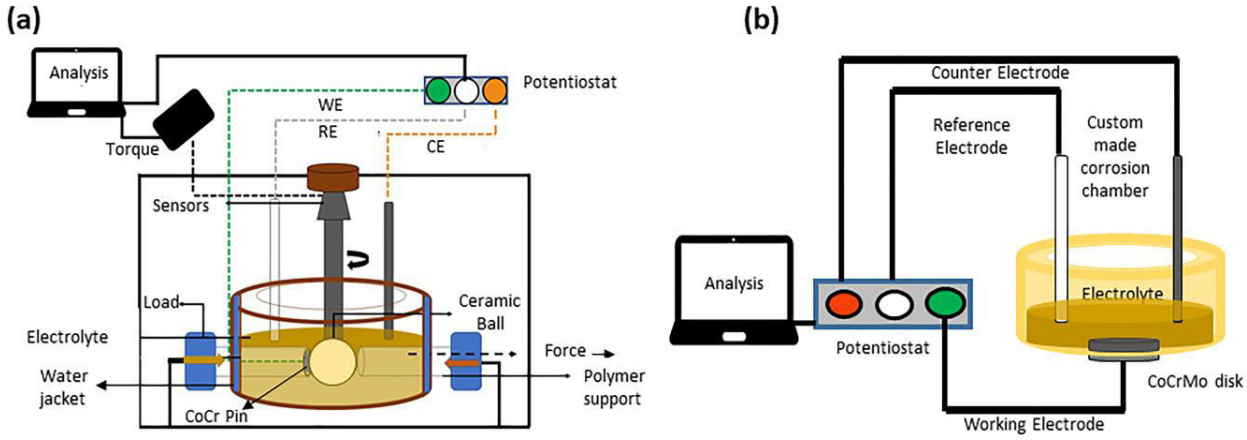

Figure 1: Schematic of the tribocorrosion hip simulator and characterization of wear particles.

a) Custom-made hip simulator to generate wear particles under physiological conditions. b) The typical set-up of corrosion apparatus connected to a potentiostat through a three-electrode system, wherein the CoCrMo disc prototype is the working electrode in contact with the electrolyte solution. Various types of media were used as the electrolyte solution while performing the electrochemical analyses.

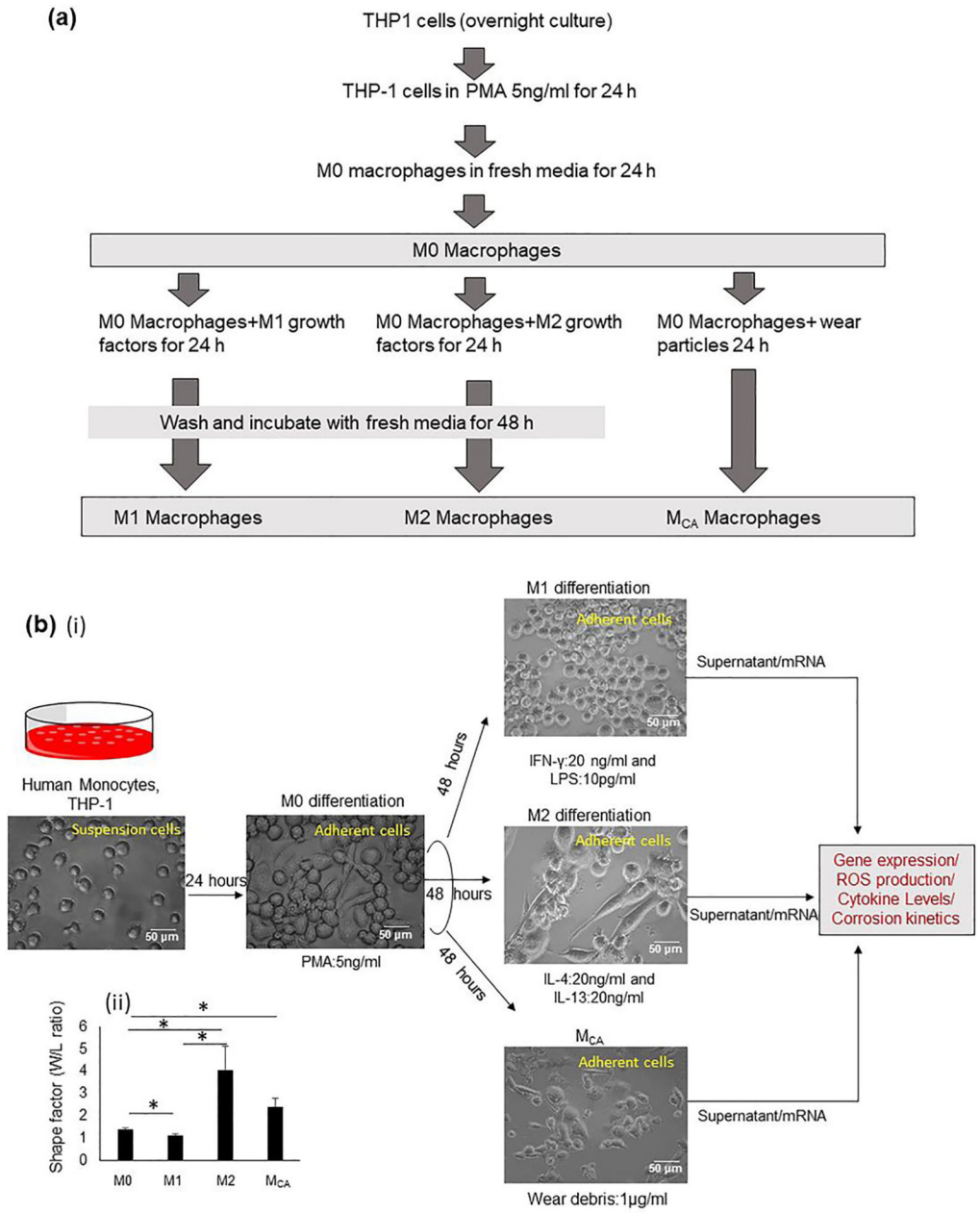

Figure 2:

a) Schematic representation of macrophage differentiation procedure**. b)(i) Microscopic evaluation of THP-1 monocyte cells**, **M0, M1, M2, and M_{CA} macrophages**. Microscopic images show that M0 macrophages exhibit adherent and spreaded morphological features after 24 hours of PMA treatment. M1 differentiation causes a circularized phenotype and M2 macrophages showed spindled-shape fibroblast-like morphology. M_{CA} cells exhibit circular and spindle-shaped cell morphology. (ii) Graph showing the shape factor (W/L ratio) of cells at different conditions.

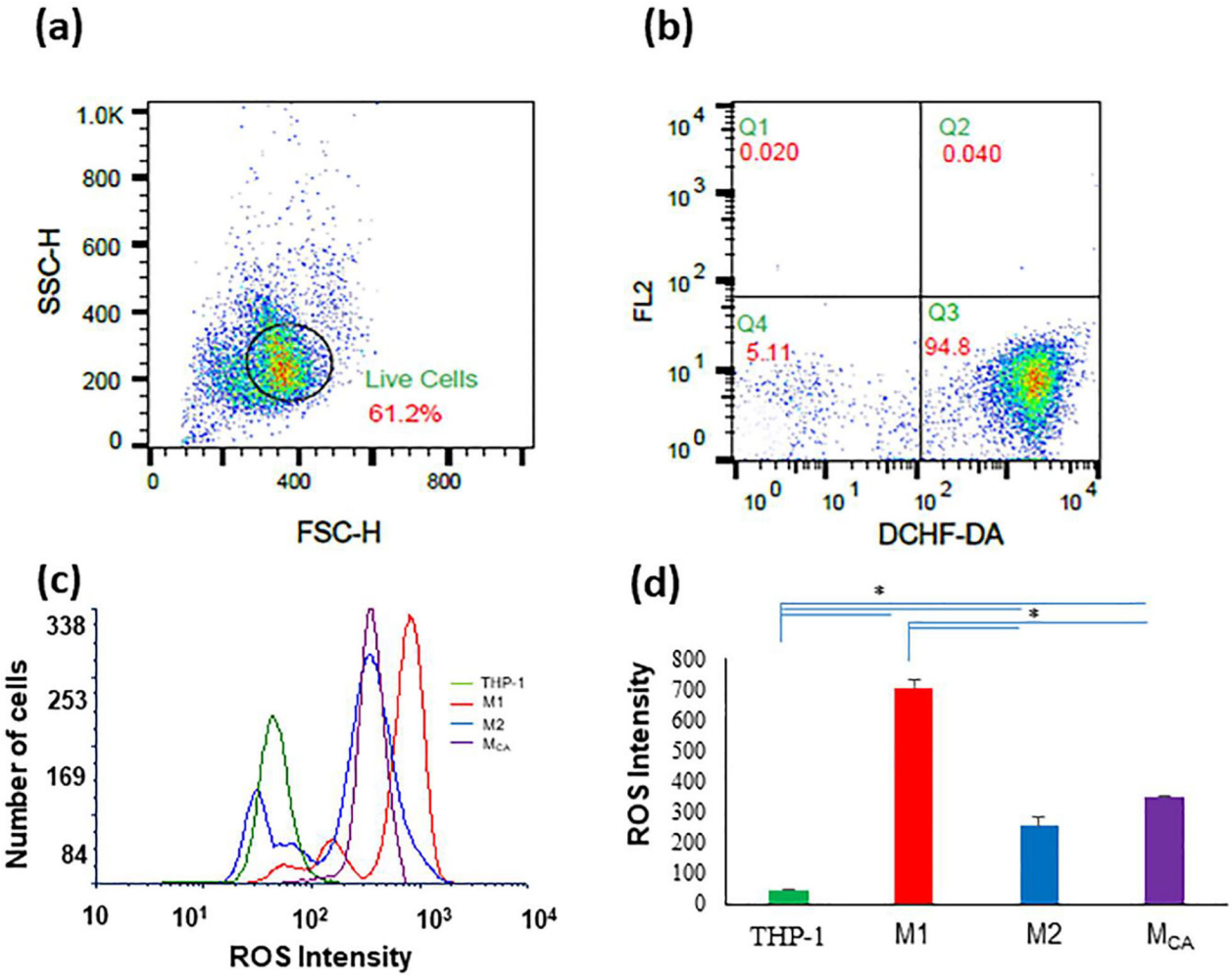

Figure 3: Reactive oxygen species (ROS) assays for THP-1, M1, M2, and M_{CA}.

Increased ROS intensity is observed with M1 macrophages, compared to M2 macrophages. (a) Representative cytogram of the live gated population of macrophages and (b) their ROS intensity by DCHF-DA vs FL2 channel. (c) Graphic representation of ROS intensity measured from the flow cytogram after 3 hours. (d) Histogram clearly depicting differences in ROS intensity between cell types. THP-1 represents untreated monocytes. Experiments were repeated three times with triplicates. * $p<0.05$ (Student's t-test).

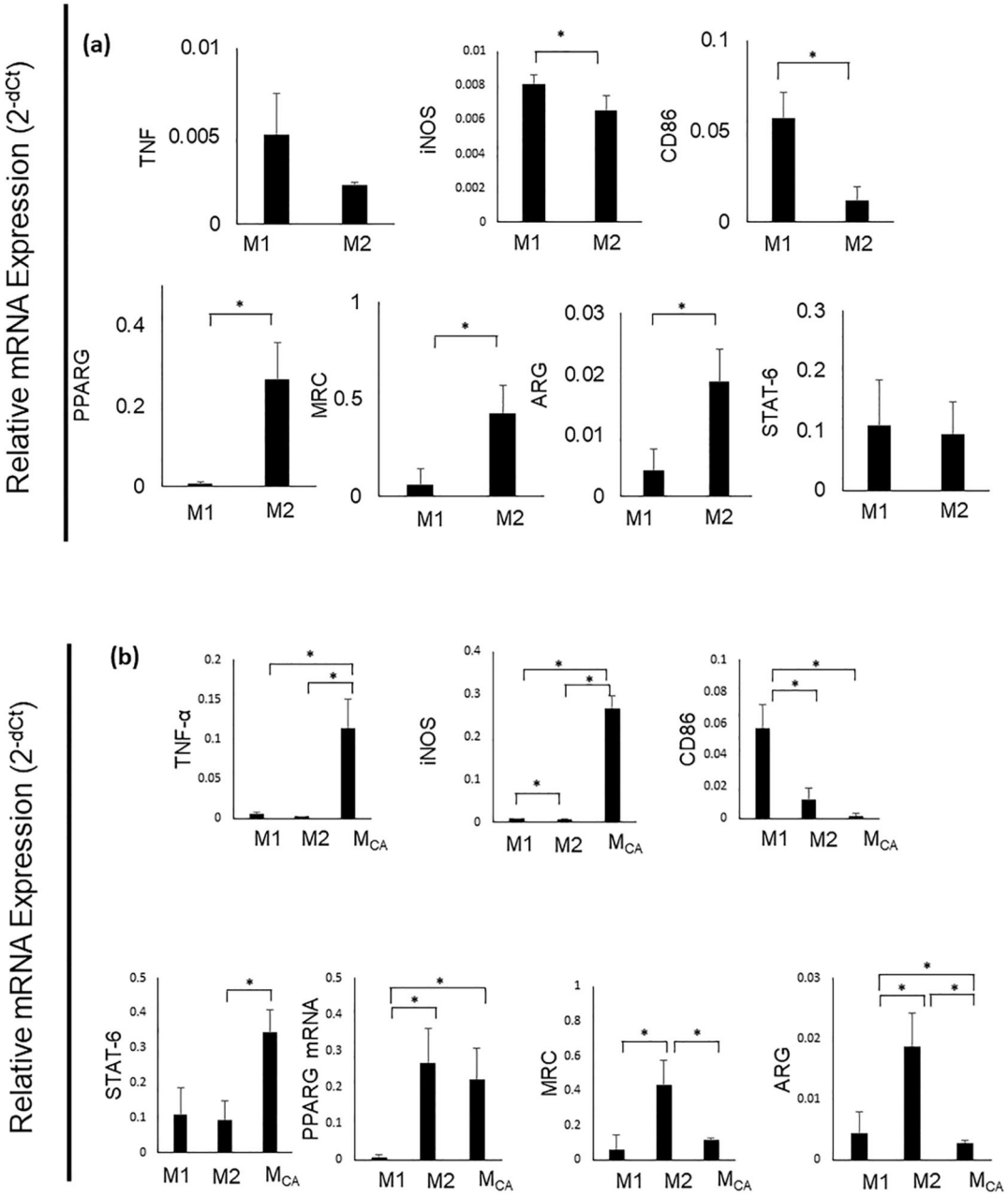

Figure 4: mRNA expression profiles for M1- and M2-specific macrophage marker genes of M1, M2, and M_{CA} macrophages.

Relative mRNA expression after 24 hours of (a) M1-specific marker genes (TNF-α, iNOS, and CD86) and M2-specific marker genes (STAT-6, PPARG, MRC, and ARG) in M1, M2 (b) M_{CA} cells in comparison to M1 and M2. All mRNA expression levels were normalized to GADPH mRNA expression. Data are the means and standard deviations of six experiments with triplicates. * $p<0.05$ (Student's t-test).

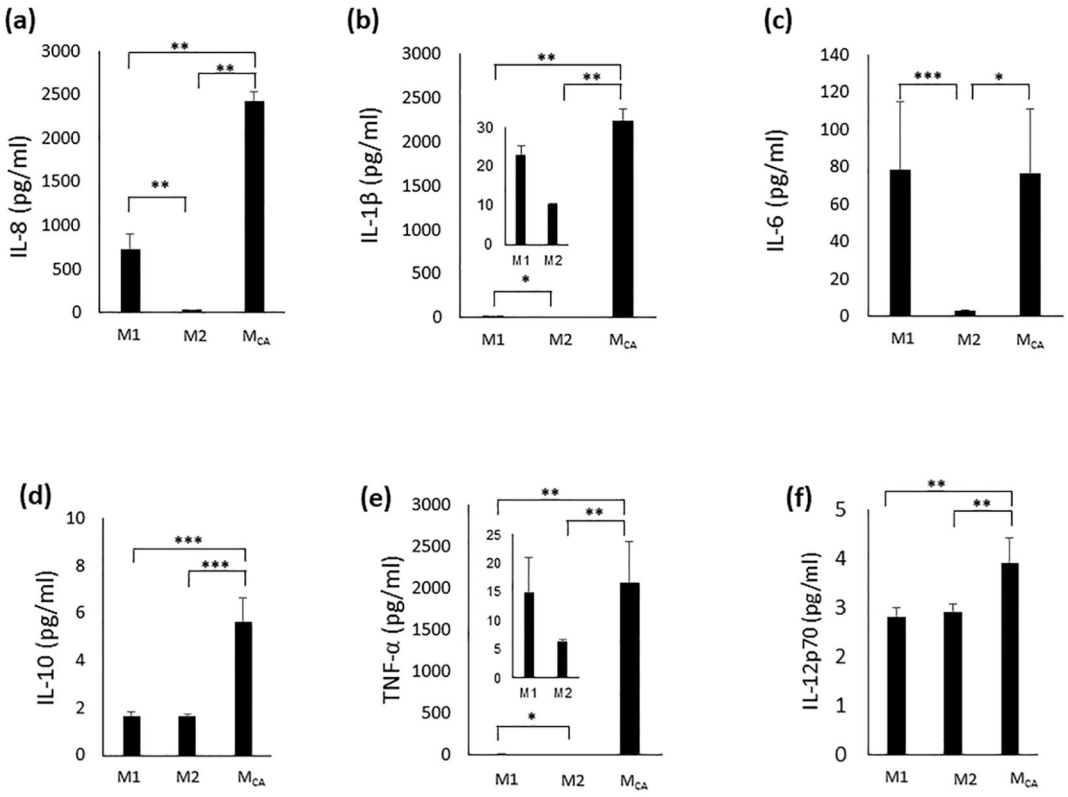

Figure 5. Cytometric bead array results of cytokines released from M1, M2, and M_{CA} macrophages.

(a-f) Bar graphs showing concentrations of cytokines released from M_{CA} macrophages, compared to concentrations released from M1 and M2 macrophages. Data are the means and standard deviations of six experiments with duplicates. * $p<0.05$, ** $p<0.01$, and *** $p<0.001$ (Student t-test).

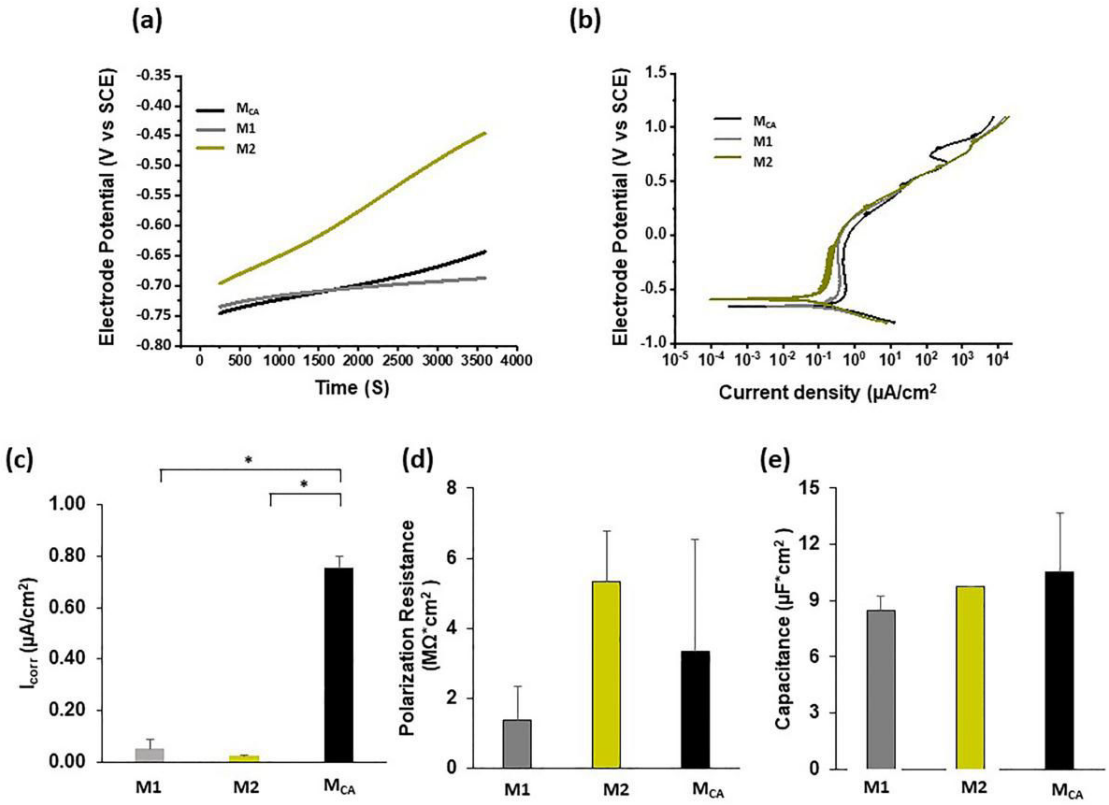

Figure 6: Electrochemical analysis of secretory products of M1, M2, and M_{CA} macrophages.

a) Graph showing open circuit potential Vs time of different media conditions. b) Tafel's plot (cyclic polarization) and c) I_{corr} values obtained by extrapolating the x-axis of Tafel's plot. d) Resistance to polarization and (e) capacitance obtained by EIS modeling by equivalent circuit. Data are the means and standard deviations of three experiments. * $p<0.05$ (Student's t-test). SCE = standard calomel electrode (the reference electrode).

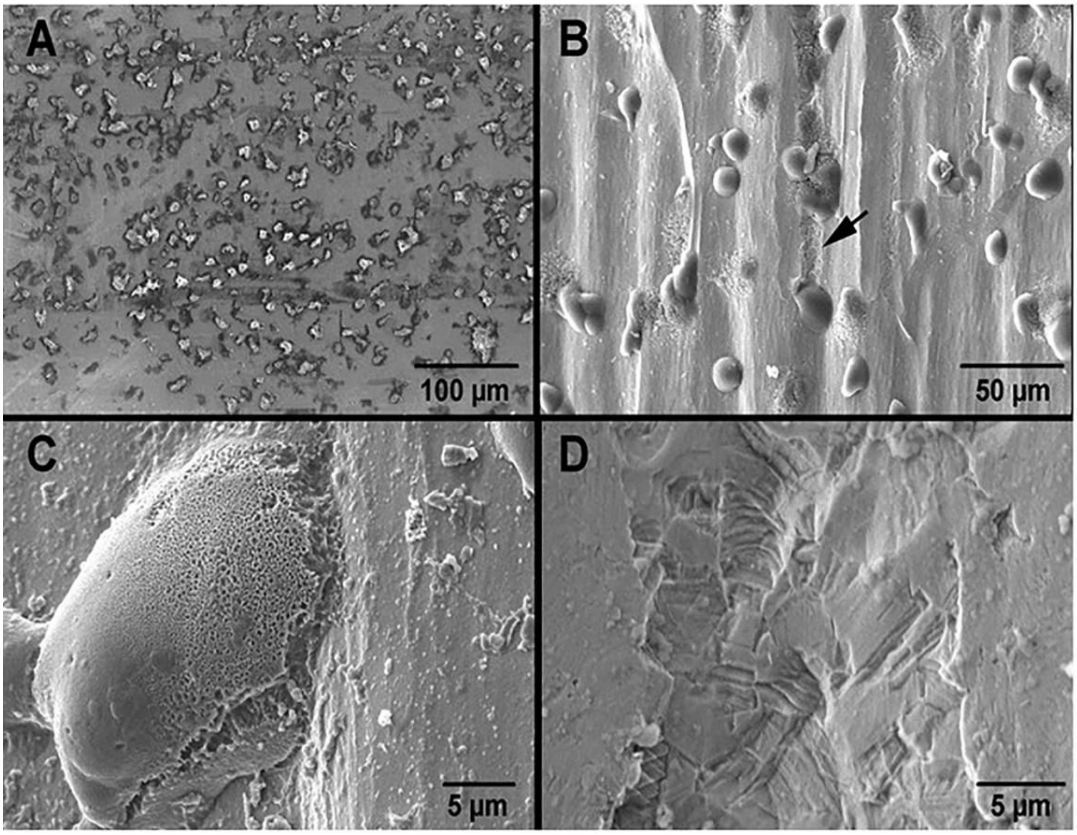

Figure 7: Secondary electron emission SEM images of a severely corroded head taper surface from a retrieved modular femoral head composed of wrought CoCrMo alloy.

A) Overview image of an area covered with multiple cell-like features. Size and morphology of these features are indicative of macrophages. It can be seen that cells charge during scanning (10kv, X250). B) Close-up image of a group of cells after gold sputtering. Cells do not charge, and greater detail of their morphology is visible. Some cells seem to leave a trail as indicated by the arrow (20kv, X500, Au/Pd coating approximately 4nm thick). C) Close-up image of a single cell after gold sputtering. The cell appears firmly attached. The fact that the cell did not lose its morphology is likely related to an immediate immersion into formalin at the time of revision surgery (5kv, X3500, Au/Pd coating approximately 4nm thick). D) Close-up image of a trail left by a cell. Typical microstructural features of wrought CoCrMo alloy can be seen such as twin boundaries and slip bands (10kv, X4300).

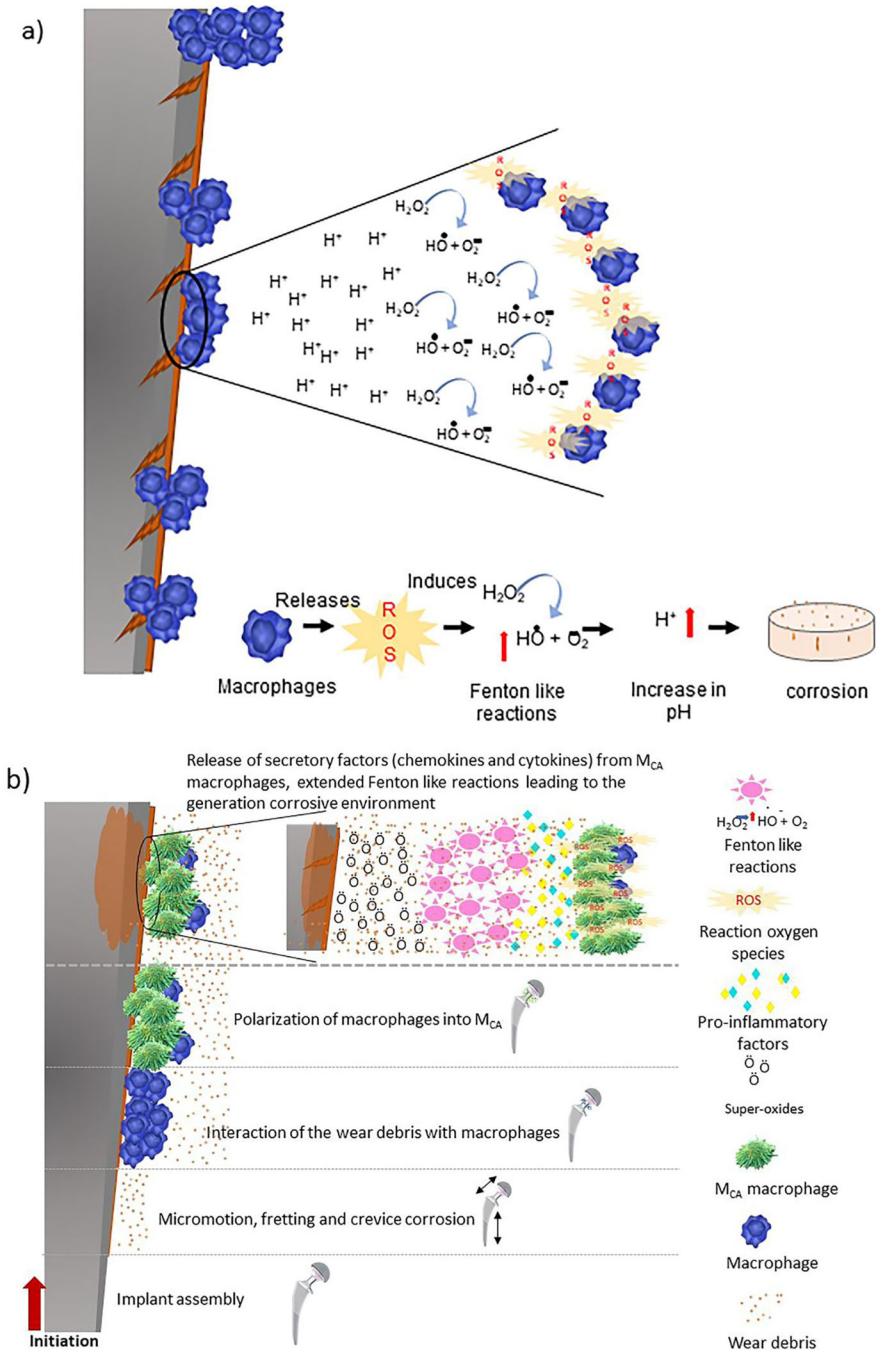

Figure 8: Schematic representation of cell-accelerated corrosion (CAC): what we knew and what we have learned.

a) Previous theory showing immune cells (possibly macrophages) producing reactive oxygen species (ROS) that lead to a Fenton-like reaction and associated pit formation on the metal implant. b) Current proposed mechanism of CAC. The mechanism starts with fretting corrosion, followed by micromotion at the head-taper interface during daily patient activities. This leads to the generation of CoCrMo wear nanoparticles at the interface, attracting monocytes and macrophages to the site. The wear particles will polarize macrophages towards M_{CA}, with a unique cytokine and chemokine profile and capacity to

generate ROS. Fenton-like reactions occurring in this altered biological environment produced by M_{CA} macrophages will produce substantial changes in the electrochemical behavior of CoCrMo at the cell-material interface, leading to accelerated corrosion.